https://doi.org/10.2352/ISSN.2470-1173.2019.10.IQSP-304

A Referenceless Image Quality Assessment Based on BSIF, CLBP, LPQ, and LCP Texture Descriptors

Pedro Garcia Freitas, Luísa Peixoto da Eira, Samuel Soares Santos, Mylène Christine Queiroz de Farias; University of Brasília; Brasília, Brazil

Abstract

In the last decades, many researchers have developed algorithms that estimate the quality of a visual content (videos or images). Among them, one recent trend is the use of texture descriptors. In this paper, we investigate the suitability of using Binarized Statistical Image Features (BSIF), the Local Configuration Pattern (LCP), the Complete Local Binary Pattern (CLBP), and the Local Phase Quantization (LPQ) descriptors to design a referenceless image quality assessment (RIQA) method. These descriptors have been successfully used in computer vision applications, but their use in image quality assessment has not yet been thoroughly investigated. With this goal, we use a framework that extracts the statistics of these descriptors and maps them into quality scores using a regression approach. Results show that many of the descriptors achieve a good accuracy performance, outperforming other state-of-the-art RIQA methods. The framework is simple and reliable.

Introduction

In many multimedia applications, image contents are altered during transmission, enhancement, and compression stages. These modifications often insert visible impairments that may be perceived by human observers. Therefore, the development of techniques that are able to predict the visual quality, as perceived by human observers, can lead to substantial advances in multimedia applications. Objective image quality assessment (IQA) models are frequently deployed in such settings to predict visual quality automatically.

Objective IQA methods can be classified according to the amount of available reference information they require. If a pristine content (reference) is required to estimate quality, the method is classified as full-reference (FR). If the method only requires a limited amount of information regarding the reference image, the method is classified as a reduced-reference (RR) method. Since requiring full or limited reference information can be a severe impediment for some applications, the solution is to adopt no-reference (referenceless) methods, which assess the quality of images with no information about the reference [1].

Referenceless IQA (RIQA) methods are broadly classified into two categories, namely distortion-specific (DS) and general-purpose (GP). DS methods include approaches that assess the visual quality impaired by a specific known distortion types, such as ringing [2], compression [3], or blockiness [4] artifacts. Although DS models can be suitable in specific contexts, these models are difficult to generalize to other distortion types. On the other hand, GP methods demand no prior knowledge about the artifact type, being, therefore, more suitable for diverse multimedia scenarios. As expected, designing GP methods is more challenging [1].

GP methods can be modeled using purely data-driven approaches based on the extraction of low-level image features, which are then mapped to subjective image quality scores using regression. GP methods can also be designed considering natural scene statistics (NSS), which models the statistics of natural images (without distortions) and quantify the severity of the distortion by measuring the degree of "unnaturalness" caused by the presence of distortions [5, 6, 7]. NSS-based methods can extract features in different domains, such as discrete cosine transform (DCT) domain [8, 9], discrete wavelet transform (DWT) domain [10, 11], spatial domain [12], etc. More recently, convolutional neural networks (CNN) have also been used in the design of NR-IQA methods [13].

Recent studies that show that visible impairments alter the statistics of texture descriptors [14]. This work was inspired by some quality-aware texture descriptors that have recently been proposed for quality assessment purposes, which include the Local Variant Patterns (LVP) [15], the Orthogonal Color Planes Patterns (OCPP) [16], and the Salient Local Binary Patterns [17, 18]. In this paper, we investigate the use of four different descriptors in the design of RIQA methods: the Complete Local Binary Pattern (CLBP), the Local Configuration Pattern (LCP), the Local Phase Quantization (LPQ), and the Binarized Statistical Image Features (BSIF) descriptors. A ML framework is used to analyze the performance of these four descriptors for the RIQA application. More specifically, we tested several combinations of the statistics extracted by these descriptors as feature vectors for a random forest regression algorithm [19].

A Brief Review of Texture Descriptors

Texture descriptors are algorithms that characterize visual features related to textures. Among the available texture descriptors, the Local Binary Pattern (LBP) is arguably one of the most successfully texture descriptors. Its sucess is due to the simplicity of the LBP model, which describes the local textures of an image by performing simple operations while achieving high performance on many texture-based problems. Formerly proposed by Ojala *et al.* [21], LBP takes the following form:

$$LBP_{R,P}(I_c) = \sum_{p=0}^{P-1} S(I_p - I_c)2^p, \tag{1}$$

where $S(t) = 1$ for $t \geq 0$ and $S(t) = 0$ otherwise. In eq. 1, $I_c = I(x,y)$ is an arbitrary central pixel at the position (x,y), $I_p = I(x_p,y_p)$ is a neighboring pixel surrounding I_c. The neighboring positions are given by $x_p = x + R\cos(2\pi p/P)$ and $y_p = y - R\sin(2\pi p/P)$, where P is the total number of neighboring pixels I_p, sampled with a distance R from I_c.

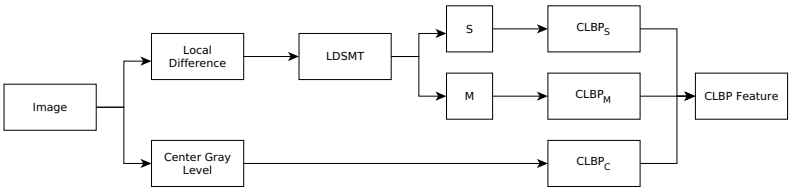

Figure 1: Framework of CLBP descriptor [20].

Although effective for many texture-based applications, the LBP does not have a good perfromance in some applications. Therefore, LBP variants have been proposed to better adapt it for these applications. In this paper, we investigate the suitability of the BSIF, the CLBP, the LPQ, and the LCP descriptors in the design of referenceless image quality assessment methods. These variantes were chosen based on recent studies that suggests that NRIQA methods using these descriptors have a high correlation with subjective quality scores [14].

Complete Local Binary Patterns (CLBP)

The LBP descriptor considers only the local differences of each pixel and its neighbors. Additionally, the complete local binary patterns consider both signs (S) and magnitude (M) of the local differences, as well as the original intensity value of the center pixel [20]. Therefore, the CLBP feature is a combination of three descriptors, namely $CLBP_S$, $CLBP_M$, and $CLBP_C$. Fig. 1 illustrates the computation of the CLBP feature.

The $CLBP_S$ and $CLBP_M$ components are computed using the local difference sign-magnitude transform (LDSMT), which is defined as $LDSMT_p = s_p \cdot m_p$, where $s_p = S(I_p - I_c)$ and $m_p = |I_p - I_c|$. The s_p is the sign descriptor used to compute $CLBP_S$, i.e. $CLBP_S$ is the same as the original LBP and it is used to code the sign information of the local differences. $CLBP_M$ is used to code the magnitude information of local differences:

$$CLBP_M = \sum_{p=0}^{P-1} \tau(m_p, c) \cdot 2^p, \tag{2}$$

where $\tau(x,c) = 1$ if $x \geq c$ and $\tau(x,c) = 0$, otherwise. Specifically, c is a threshold set as the mean value of the input image I. Finally, the $CLBP_C$ is used to code the information of original center gray level value $CLBP_C = \tau(I_c, c)$. The three descriptors, $CLBP_S$, $CLBP_M$, and $CLBP_C$, are combined. Individual histograms are computed and concatenated. This joint histogram is used as a CLBP feature.

Local Configuration Patterns (LCP)

LCP [22] decomposes the image information into two levels: local structural information and microscopic configuration information. The local structural information is composed by LBP features, while the microscopic configuration (MiC) information is determined by the image configuration and the pixel-wise interaction relationships. MiC is modeled by estimating the optimal weights of the neighboring pixel intensities, which helps to reconstruct the central pixel intensity linearly. The reconstruction error E is defined by:

$$E(w_0, w_1, \cdot, w_{P-1}) = \left| I_c - \sum_{p=0}^{P-1} w_p I_p \right|, \tag{3}$$

where w_p are weighting parameters associated with neighboring pixel I_p. Least square (LS) techniques are used to find the minimal reconstruction error and to select the optimal parameters. The optimal parameter W_L is given by:

$$W_L = \left(V_L^T V_L \right)^{-1} V_L^T C_L, \tag{4}$$

where C_L is the LS problem and V_L is the neighbouring pixel intensities. Rotation invariant features are obtained by applying the Fourier transform to the optimal parameter W_L:

$$H_L(k) = \sum_{p=0}^{P-1} W_L(i) \cdot e^{\frac{-j2\pi kp}{P}}. \tag{5}$$

$|H_L|$ gives the MiC feature that encodes the pixel-wise interaction relationships and the local contrast of each pattern.

Local Phase Quantization (LPQ)

LPQ [23] performs a quantization of the Fourier transform phase in local neighborhoods. Assuming that $G(u)$ and $F(u)$ are the discrete Fourier transforms (DFT) of the blurred $g(z)$ and original $f(z)$ images, which are related $G(u) = F(u) \cdot H(u)$. Assuming that $h(x) = h(-x)$, its DFT is always real and the phase assumes only two values, namely:

$$\angle H(u) = \begin{cases} 0, & H(u) \geq 0 \\ \pi, & \text{otherwise.} \end{cases} \tag{6}$$

For the LPQ descriptor, the phase is computed in the local neighborhood N_z, for each pixel position of $f(z)$. The local spectrum is computed with the following equation:

$$F(u,x) = \sum_{y \in N_z} f(y) \cdot w_R(y-x) \cdot e^{-j2\pi uy}, \tag{7}$$

where u is the frequency and w_R is a window given by:

$$w_R(x) = \begin{cases} 1, & |x| < \frac{N_R}{2} \\ 0, & \text{otherwise.} \end{cases} \tag{8}$$

The local Fourier coefficients are computed at four frequencies for each pixel position, i.e., $F(x) = [F(u_1,x), F(u_2,x), F(u_3,x), F(u_4,x)]$, where $u_1 = [a,0]^T$, $u_2 = [0,a]^T$, $u_3 = [a,a]^T$, and $u_4 = [a,-a]^T$. In these cases, a is sufficiently small to satisfy $H(u_i) > 0$. The phase of the Fourier coefficients is given by the signs of the real and imaginary parts of each component $F(x)$, computed by scalar quantization, i.e., $q_j = 1$ if $g_j \geq 0$ and $q_j = 0$ otherwise. Specifically, g_j is the j-th component of $G(x) = [Re\{F(x)\}, Im\{F(x)\}]$. After generating the binary coefficients q_j, the feature vector is generated using the same technique used in the LBP.

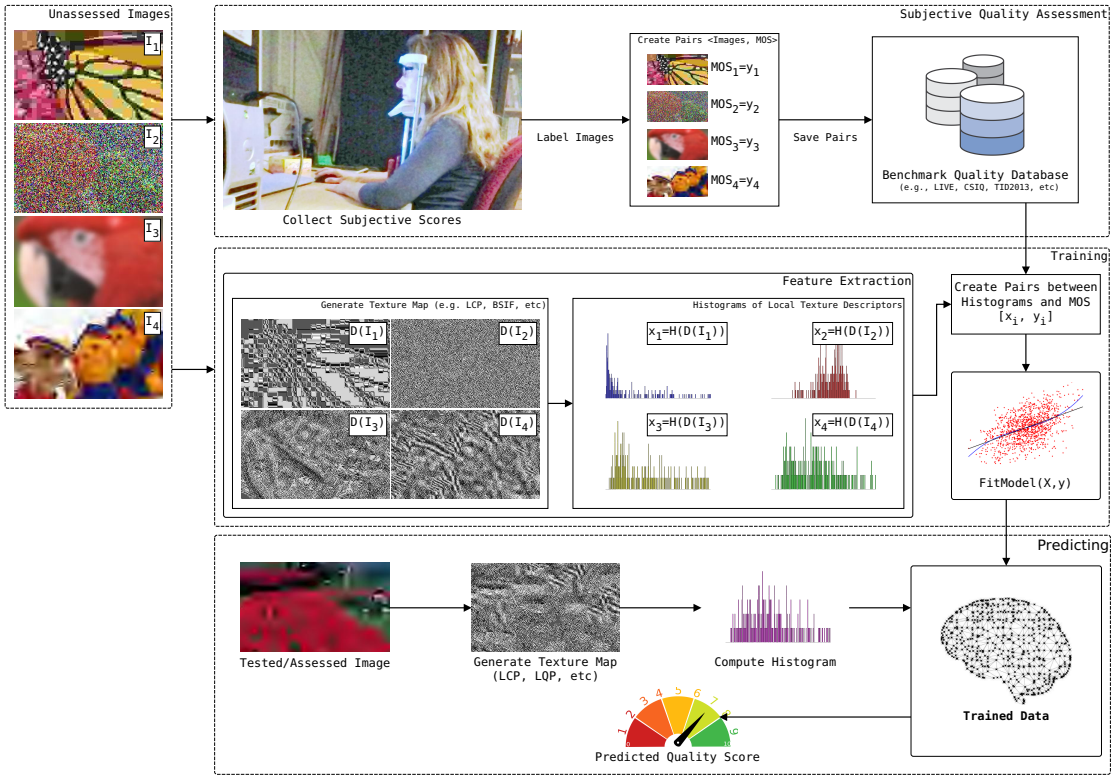

Figure 2: Framework of the proposed referenceless image quality assessment methodology.

Binarized Statistical Image Features (BSIF)

Differently from previous descriptors, which operate on pixels, BSIF [24] works on patches of pixels. Given an image patch X of size $l \times l$ pixels and a linear symmetric filter W_i of the same size, the filter response s_i is computed as follows:

$$s_i = \sum_{u,v} W_i(u,v)X(u,v) = w_i^T x, \tag{9}$$

where vectors w and x contain the pixels of W_i and X, respectively. The binarized feature b_i is 1 if $s_j > 0$ and 0 otherwise.

The filters W_i are learned via independent component analysis (ICA). The binarized features b_i are aggregated following the same procedure described for generating the LBP labels. The descriptive features are obtained by computing the histogram of the aggregated data.

Proposed Framework

In the previous section, we presented four texture descriptors, which were designed for pattern recognition and computer vision applications. Our goal is to investigate if these descriptors are suitable for image quality assessment, more specifically to RIQA applications. Moreover, we are interested in understanding the relationship between the type of descriptor and the accuracy performance of the corresponding RIQA method.

Figure 2 depicts the overall framework of the proposed RIQA method, which is composed of a training stage and a predicting stage. In the training stage, we use a set of pristine and degraded images, with the corresponding subjective quality scores. These quality scores, often called mean observer scores (MOS), are obtained by performing psychophysical experiments with voluntary participants, who rate the quality of each image in the database. This labeled database, which is composed by pairs of test images and their corresponding MOS values, is used as an entry to the training stage. In this work, we will refer to the *k-th* image as I_k and to the associated MOS value as v_k.

For each pair (I_k, v_k) of the labeled database, the training stage extracts the image features to generate the IQA model. More specifically, for each image I_k, we apply a given LPB-variant operator and, then, compute the histogram H_k of the resulting outputs. Then, we concatenate all histograms to produce the corresponding feature vector. Therefore, the training data is composed by a pair (H_k, v_k) for each image I_k, resulting in a matrix $H \in \mathbb{R}^{K \times Q}$ and a vector $v \in \mathbb{R}^{1 \times K}$, where K is the number of training entries (rows of H) and Q is the number of features (columns and the numbers of bins of H_k).

The prediction model is built using a regression model. The model maps each H_k into a real value $\hat{v}_k$, which is a prediction of the corresponding MOS value v_k. The chosen regression model is the random forest (RF) regressor [25], since this regressor has shown a good performance in several computer vision applications. More specifically, Fernandez-Delgado *et al.* [26] conducted an exhaustive evaluation of several machine learning methods and their results showed that the RF methods have the best performance.

Finally, after the training stage obtains a prediction model, the image quality of individual images can be estimated using this model. The estimation procedure used by the predicting stage is the same used in the training stage. In other words, the predicting stage computes the same features (descriptor histograms) and uses the trained model to obtain an objective quality score $\hat{v}_k$.

Table 1: Correlation values of concatenations of the best descriptors, tested on LIVE2, CSIQ, and TID201 databases.

	LIVE2			CSIQ			TID203			Hits	
Configuration	**LCC**	**SROCC**	**KRCC**	**LCC**	**SROCC**	**KRCC**	**LCC**	**SROCC**	**KRCC**	**DIS**	**ALL**
BSIF (1)	0.93261	0.93473	0.78654	0.82886	0.79092	0.60667	0.72834	0.65033	0.47632	0	0
CLBP (2)	0.92709	0.92698	0.77503	0.81665	0.77059	0.58061	0.70064	0.62889	0.45709	8	0
LCP (3)	0.91648	0.91455	0.75519	0.82118	0.76454	0.57751	0.70448	0.61048	0.43924	8	0
LPQ (4)	0.92312	0.91675	0.75803	0.80444	0.76039	0.58050	0.71746	0.65445	0.47403	3	0
1 & 2	0.93170	0.93393	0.78673	0.84318	0.81004	0.62461	0.74796	0.68459	0.50275	3	0
1 & 3	0.93742	**0.94181**	**0.79911**	0.84879	0.80897	0.62734	0.72941	0.64007	0.46964	14	2
1 & 4	0.93820	0.93186	0.78365	0.82930	0.79105	0.61037	0.72579	0.65303	0.48100	2	0
1 & 4	0.92585	0.93408	0.78460	0.84499	0.79189	0.60767	0.76157	0.67323	0.49396	8	0
2 & 4	0.93616	0.92713	0.77488	0.84451	0.80021	0.61818	0.72828	0.66646	0.48620	0	0
3 & 4	0.92809	0.92538	0.77098	0.84060	0.79503	0.61285	0.74430	0.68124	0.49723	6	0
1,& 2 & 3	0.93551	0.94099	0.79866	0.84599	0.81246	0.63158	0.75316	0.67277	0.49396	**22**	0
1 & 2 & 4	**0.94533**	0.93625	0.79035	0.84796	0.81411	0.63121	0.74956	0.68594	0.50570	11	1
1 & 3 & 4	0.94157	0.93741	0.79117	0.84781	**0.81422**	**0.63393**	0.74399	0.67418	0.49388	6	2
2 & 3 & 4	0.93474	0.93086	0.77992	**0.85347**	0.80860	0.62819	**0.76518**	**0.70536**	**0.51960**	15	**4**
1& 2 & 3 & 4	0.94014	0.93707	0.79208	0.85114	0.81332	0.63199	0.68572	0.64534	0.48200	8	0

Simulation Results

Each of the tests reported in this work corresponded to 1,000 simulations. For each simulation, we computed the linear correlation coefficient (LCC), the Spearman's rank correlation coefficient (SROCC), and the Kendall rank correlation coefficient (KRCC) between the quality predictions produced by the objective methods and the corresponding subjective scores (MOSs). We report the average of these correlation coefficients over all simulations. We also computed the variation of these coefficients, which are not reported here since the results were mostly constant. The tests were performed using 3 popular image quality databases:

- LIVE2 [27]: This database has 982 test images, including 29 originals. This database includes 5 categories of distortions: JPEG, JPEG 2000 (JPEG2k), white noise (WN), Gaussian blur (GB), fast fading (FF).
- CSIQ [28]: This database has a total fo 866 test images, consisting of 30 originals and 6 different categories of distortions. The distortions include JPEG, JPEG 2000 (JPEG2k), JPEG, white noise (WN), Gaussian blur (GB), fast fading (FF), global contrast decrements (CD), and additive Gaussian pink noise (PN).
- TID2013 [29]: This database contains 25 reference images with the following distortions: Additive Gaussian noise (AGN), Additive noise in color components (AGC), Spatially correlated noise (SCN), Masked noise (MN), High frequency noise (HFN), Impulse noise (IN), Quantization noise (QN), Gaussian blur (GB), Image denoising (ID), JPEG, JPEG2k, JPEG transmission errors (JPEGTE), JPEG2k transmission errors (JPEG2kTE), Non eccentricity pattern noise (NEPN), Local block-wise distortions (LBD), Intensity shift (IS), Contrast change (CC), Change of color saturation (CCS), Multiplicative Gaussian noise (MGN), Comfort noise (CN), Lossy compression (LC), Image color quantization with dither (ICQ), Chromatic aberration (CA), and Sparse sampling and reconstruction (SSR).

For each of the databases, we report the average correlation coefficients (over 1,000 simulations) for each of the distortion types and for the complete database (ALL).

For each of the four descriptors (CLBP, LCP, LPQ, and BSIF), we tested several different configurations of parameters to find out which configuration had the best accuracy performance. To select the best configuration, we counted the number of hits, where a hit corresponded to a particular configuration that obtained the best result either in terms of LCC, SROCC, and KRCC values for the complete database (ALL). The best configuration was the one who got the highest number of hits in terms for the 3 correlation coefficients and the 3 complete databases (the maximum number of hits is 9, since there are 3 databases and 3 coefficients). In addition, we also computed the number of hits for each individual distortion (DIS) for the 3 databases. We chose 2 more configurations, which corresponded to the configurations with the first and second highest number of DIS hits.

After establishing the 3 best configurations of parameters for each of the four descriptors, these configurations were concatenated and re-tested. More specifically, for each descriptor, the feature vectors of the 3 best configurations were combined in all 4 possible ways and re-tested. Again, we compared the results (4 concatenations of the 3 individual configurations) by counting the number of hits of the 3 correlation coefficients for the 3 complete databases (ALL). The results obtained in these sets are summarized as follows.

- The chosen CLBP combination was the pair $CLBP_S$ and $CLBP_M$, with uniform local and rotation invariance. For this CLBP combination, the 3 best configurations were: ($R = 1$, $P = 4$), ($R = 1$, $P = 8$), and ($R = 2$, $P = 12$). The single best concatenation was the combination of ($R = 1$, $P = 8$) and ($R = 1$, $P = 4$).
- The 3 best LCP configurations were: ($R = 1$, $P = 4$, uniform local and rotation invariance mapping), ($R = 1$, $P = 8$, rotation invariance mapping), and ($R = 2$, $P = 16$, uniform local and rotation invariance mapping). The single best concatenation was the combination of ($R = 1$, $P = 8$, rotation invariance mapping) and ($R = 2$, $P = 16$, uniform local and rotation invariance mapping).
- For LPQ, we compared 3 different methods for local frequency estimation: Guassian Derivative Quadrature, STFT with Gaussian Window and STFT with Uniform Window (basic version of LPQ). As there were only 3 options, we concatenated them and obtained the best results with the concatenation of the 3 possibilities.
- We tested 8 different versions of BSIF: (1) 3x3 patch with 5 bits, (2) 3x3 patch with 6 bits, (3) 3x3 patch with 7 bits, (4) 3x3 patch with 8 bits, (5) 5x5 patch with 9 bits, (6) 5x5 patch with 10 bits, (7) 5x5 patch with 11 bits, and (8) 7x7 patch with 12 bits. The 3 best single configurations were 4,

7, and 8. When we tested all concatenations, we found that the best was the one of (4) and (7).

Lines 2-5 in Table 1 show the correlation coefficients and hit counts obtained for the best configurations of BSIF, CLBP, LCP, and LPQ, as discussed above. In this table, numbers in bold represent the highest values of a column.

Having established the best concatenation for each descriptor, we once again concatenated and tested the feature vectors of the best overall concatenations of the 4 descriptors (Lines 2-5 in Table 1). A total of 11 combinations of the best concatenated descriptors were tested. Again, we compared the amount of hits for the 3 databases (ALL) to choose the best overall combination of the 4 descriptors. Lines 6-16 in Table 1 show results obtained for several concatenations of BSIF, CLBP, LCP, and LPQ. Notice that the overall best combination was "2& 3& 4", which corresponds to a combination of the best configurations of CLBP, LCP, and LPQ (line 15 of Table 1). This specific configuration will be referred as the 'proposed method' in the rest of the paper.

Table 2 compares the proposed method with other state of the art IQA methods. In this table, numbers in italics represent the IQA method with the best overall performance (in terms of correlation), whilst numbers in bold correspond to the referenceless IQA method with the best performance. This table presents the results for the complete database (ALL) and each type of distortion. As before, the first two hit counts take into account all IQA methods, while the last two hit counts take into account only the referenceless IQA methods. We can see that, for the TID2013 database, the proposed method achieves the best overall results (hits ALL) and obtains 9 DIS hits. It is worth pointing out that TID2013 is the most diverse database of the set of databases. Although the proposed method does not have the best SROCC on the other databases, the difference from the best result is only 0.0183 for LIVE2 and 0.1056 for CSIQ (considering the ALL case), proving that the method has a competitive performance.

Conclusions

We proposed a ML method for RIQA, which is based on combinations of texture descriptors. Our results show that the proposed method is able to achieve a good correlation with subjective quality scores, specially in more diverse contents. The ML framework used to test the descriptors is generic and can be adapted to be used for other types of feature extractors, being therefore suitable for general multimedia applications. Future works include an investigation of the suitability of the proposed framework for video quality assessment (VQA) applications.

Acknowledgments

This work was supported by the Fundação de Apoio a Pesquisa do Distrito Federal (FAP-DF), by the Coordenação de Aperfeiçoamento de Pessoal de Nível Superior (CAPES), the Conselho Nacional de Desenvolvimento Científico e Tecnológico (CNPq), and by the University of Brasília (UnB).

References

[1] Damon M Chandler. Seven challenges in image quality assessment: past, present, and future research. *ISRN Signal Processing*, 2013, 2013.

[2] Xiaojun Feng and Jan P Allebach. Measurement of ringing artifacts in jpeg images. In *Digital Publishing*, volume 6076, page 60760A. International Society for Optics and Photonics, 2006.

[3] S Alireza Golestaneh and Damon M Chandler. No-reference quality assessment of jpeg images via a quality relevance map. *Signal Processing Letters, IEEE*, 21(2):155–158, 2014.

[4] Hugo Tadashi M Kussaba and Mylene CQ Farias. Blind estimation of blocking artifacts in digital videos. *Latin Display*, 2010, 2010.

[5] Anush Krishna Moorthy and Alan Conrad Bovik. Blind image quality assessment: From natural scene statistics to perceptual quality. *IEEE transactions on Image Processing*, 20(12):3350–3364, 2011.

[6] Anish Mittal, Rajiv Soundararajan, and Alan C Bovik. Making a" completely blind" image quality analyzer. *IEEE Signal Process. Lett.*, 20(3):209–212, 2013.

[7] Yi Zhang, Anush K Moorthy, Damon M Chandler, and Alan C Bovik. C-diivine: No-reference image quality assessment based on local magnitude and phase statistics of natural scenes. *Signal Processing: Image Communication*, 29(7):725–747, 2014.

[8] Lin Ma, Songnan Li, and King Ngi Ngan. Reduced-reference image quality assessment in reorganized dct domain. *Signal Processing: Image Communication*, 28(8):884–902, 2013.

[9] Michele A Saad, Alan C Bovik, and Christophe Charrier. Blind image quality assessment: A natural scene statistics approach in the dct domain. *IEEE transactions on Image Processing*, 21(8):3339–3352, 2012.

[10] Anush Krishna Moorthy and Alan Conrad Bovik. Blind image quality assessment: From natural scene statistics to perceptual quality. *IEEE transactions on Image Processing*, 20(12):3350–3364, 2011.

[11] Lihuo He, Dacheng Tao, Xuelong Li, and Xinbo Gao. Sparse representation for blind image quality assessment. In *Computer Vision and Pattern Recognition (CVPR), 2012 IEEE Conference on*, pages 1146–1153. IEEE, 2012.

[12] Anish Mittal, Anush Krishna Moorthy, and Alan Conrad Bovik. No-reference image quality assessment in the spatial domain. *IEEE Transactions on Image Processing*, 21(12):4695–4708, 2012.

[13] Le Kang, Peng Ye, Yi Li, and David Doermann. Convolutional neural networks for no-reference image quality assessment. In *Proceedings of the IEEE conference on computer vision and pattern recognition*, pages 1733–1740, 2014.

[14] Pedro Garcia Freitas, Luísa da Eira, Samuel Santos, and Mylene Farias. On the application lbp texture descriptors and its variants for no-reference image quality assessment. *Journal of Imaging*, 4(10):114, 2018.

[15] Pedro Garcia Freitas, Welington Yorihiko Lima Akamine, and Mylène Christine Queiroz de Farias. Blind image quality assessment using local variant patterns. In *Intelligent Systems (BRACIS), 2017 Brazilian Conference on*, pages 252–257. IEEE, 2017.

[16] Pedro Garcia Freitas, Welington Yorihiko Lima Akamine, and Mylène CQ Farias. No-reference image quality assessment using orthogonal color planes patterns. *IEEE Transactions on Multimedia*, 2018.

[17] Pedro Garcia Freitas, Welington Yorihiko Lima Akamine, Mylène Christine Queiroz, et al. No-reference image quality assessment using salient local binary patterns. *Electronic Imaging*, 2018(12):367–1, 2018.

[18] Pedro Garcia Freitas, Sana Alamgeer, Welington YL Akamine, and Mylène CQ Farias. Blind image quality assessment based on multiscale salient local binary patterns. In *Proceedings of the 9th ACM Multimedia Systems Conference*, pages 52–63. ACM, 2018.

[19] Miao Liu, Mingjun Wang, Jun Wang, and Duo Li. Comparison of

Table 2: Mean SCROCC of the PSNR, SSIM, RIQMC, BRISQUE, CORNIA, CQA, SSEQ, LTP, NFERM, RIQA-SCTE [30] and the proposed metrics, obtained for 1000 simulation runs on the LIVE2, CSIQ and TID2013 databases

Database	Distortion	PSNR	SSIM	RIQMC	BRISQUE	CORNIA	CQA	SSEQ	LTP	NFERM	RIQA-SCTE	PROPOSED
LIVE2	JPEG	0.8515	0.9481	0.7794	0.8641	0.9002	0.8257	0.9122	0.9395	***0.9645***	0.9325	0.9288
	JPEG2k	0.8822	0.9438	0.5383	0.8838	0.9246	0.8366	0.9388	0.9372	0.9411	***0.9497***	**0.9186**
	WN	*0.9851*	0.9793	0.6628	0.9750	0.9500	0.9764	0.9544	0.9646	0.9838	**0.9845**	0.9685
	GB	0.7818	0.8889	0.8711	0.9304	0.9465	0.8377	0.9157	0.9530	0.9219	***0.9641***	0.9354
	FF	0.8869	*0.9335*	0.6802	0.8469	**0.9132**	0.8262	0.9038	0.8758	0.8627	0.8977	0.8615
	ALL	0.8013	0.8902	0.6785	0.9098	0.9386	0.8606	0.9356	0.9316	0.9405	***0.9492***	0.9309
CSIQ	JPEG	0.9009	0.9309	0.7242	0.8525	0.8319	0.6506	0.8066	0.9292	0.9036	***0.9331***	0.8924
	JPEG2k	*0.9309*	0.9251	0.5795	0.8458	0.8405	0.8214	0.7302	0.8877	**0.9223**	0.8871	0.8701
	WN	0.9345	0.8761	0.4678	0.6931	0.6187	0.7276	0.7876	0.6454	0.9214	***0.9346***	0.8139
	GB	*0.9358*	0.9089	0.8007	0.8337	0.8526	0.7486	0.7766	**0.9244**	0.8962	0.9197	0.8901
	PN	0.9315	0.8871	0.3653	0.7740	0.5340	0.5463	0.6661	0.7828	0.6334	***0.9461***	0.7794
	CD	0.8862	0.8128	*0.9565*	0.4255	0.4458	0.5383	0.4172	0.2082	0.3774	**0.8097**	0.3079
	ALL	0.8088	0.8116	0.5066	0.7597	0.6969	0.6369	0.7007	0.8280	***0.9142***	0.8949	0.8086
TID2013	AGC	0.8568	0.7912	0.3555	0.4166	0.2605	0.3964	0.3949	0.5963	0.7077	***0.9217***	0.6259
	AGN	*0.9337*	0.6421	0.6055	0.6416	0.5689	0.6051	0.6040	0.6631	0.8567	**0.8662**	0.8014
	CA	*0.7759*	0.7158	0.5726	**0.7310**	0.6844	0.4380	0.4366	0.6749	0.6357	0.5991	0.6018
	CC	0.4608	0.3477	*0.8044*	0.1849	0.1400	0.2043	0.2006	0.1886	0.2148	**0.7583**	0.1281
	CCS	0.6892	*0.7641*	0.0581	0.2715	0.2642	0.2461	0.2547	0.2384	0.3106	**0.5765**	0.1346
	CN	*0.8838*	0.6465	0.6262	0.2176	0.3553	0.1623	0.1642	0.3880	0.1385	0.5100	**0.6473**
	GB	*0.8905*	0.8196	0.7687	0.8063	0.8341	0.7019	0.7058	0.7465	0.8502	0.8655	**0.8904**
	HFN	0.9165	0.7962	0.4267	0.7103	0.7707	0.7104	0.7061	0.7626	0.8797	***0.9319***	0.8662
	ICQ	*0.9087*	0.7271	0.8691	0.7663	0.7044	0.6829	0.6834	0.7603	0.4804	0.7877	**0.8165**
	ID	*0.9457*	0.8327	0.8661	0.5243	0.7227	0.6711	0.6716	0.7063	0.6405	0.8388	**0.8389**
	IN	*0.9263*	0.8055	0.1222	0.6848	0.5874	0.4231	0.4272	0.6484	0.1735	0.6699	**0.8260**
	IS	0.7647	0.7411	0.5979	0.2224	0.2403	0.2011	0.2013	0.3291	0.0407	***0.8792***	0.0878
	JPEG	*0.9252*	0.8275	0.7293	0.7252	0.7815	0.6317	0.6284	0.6631	0.8711	0.6160	**0.8976**
	JPEGTE	0.7874	0.6144	0.6009	0.3581	0.5679	0.2221	0.2195	0.2314	0.1281	***0.8531***	0.6095
	JPEG2k	*0.8934*	0.7531	0.5967	0.7337	0.8089	0.7219	0.7205	0.7780	0.8068	0.3819	**0.8762**
	JPEG2kTE	*0.8581*	0.7067	0.7189	**0.7277**	0.6113	0.6529	0.6529	0.6594	0.1686	0.1754	0.7115
	LBD	0.1301	0.6213	0.2471	0.2833	0.2157	0.2382	0.2290	0.3813	0.1995	***0.9000***	0.1114
	LC	*0.9386*	0.8311	0.5346	0.5726	0.6682	0.4561	0.4460	0.6533	0.6516	**0.7738**	0.7695
	MGN	*0.9085*	0.7863	0.3751	0.5548	0.4393	0.4969	0.4897	0.6209	0.7159	0.1254	**0.7315**
	MN	0.8385	0.7388	0.0438	0.2650	0.2342	0.2506	0.2575	0.4243	0.2238	***0.8769***	0.6532
	NEPN	*0.6931*	0.5326	0.1496	0.1821	**0.2855**	0.1308	0.1275	0.1256	0.0667	0.1985	0.2146
	QN	0.8636	0.7428	0.8697	0.5383	0.4922	0.7242	0.7214	0.7361	0.7716	***0.8662***	0.8571
	SCN	*0.9152*	0.7934	0.7811	0.7238	0.7043	0.7121	0.7064	0.7015	0.2181	**0.9146**	0.8042
	SSR	0.9241	0.7774	0.6967	0.7101	0.8594	0.8115	0.8084	0.8457	0.7865	0.9023	***0.9367***
	ALL	0.6869	0.5758	0.4439	0.5416	0.6006	0.4925	0.4900	0.6078	0.3971	0.7231	***0.7652***
AVG		*0.8377*	0.7807	0.5808	0.6234	0.6262	0.5741	0.5893	0.6563	0.6084	**0.7767**	0.7134
Hits IQA	DIS	**17**	2	3	0	0	0	0	0	2	12	2
	ALL	0	0	0	0	0	0	0	0	**1**	**1**	**1**
Hits RIQA	DIS	-	-	-	2	2	0	0	1	3	**21**	10
	ALL		-	-	0	0	0	0	0	**1**	**1**	**1**

random forest, support vector machine and back propagation neural network for electronic tongue data classification: Application to the recognition of orange beverage and chinese vinegar. *Sensors and Actuators B: Chemical*, 177:970–980, 2013.

[20] Zhenhua Guo, Lei Zhang, and David Zhang. A completed modeling of local binary pattern operator for texture classification. *IEEE Transactions on Image Processing*, 19(6):1657–1663, 2010.

[21] Timo Ojala, Matti Pietikainen, and Topi Maenpaa. Multiresolution gray-scale and rotation invariant texture classification with local binary patterns. *IEEE Transactions on pattern analysis and machine intelligence*, 24(7):971–987, 2002.

[22] Guoying Zhao Yimo Guo and Matti Pietikäinen. Texture classification using a linear configuration model based descriptor. In *Proceedings of the British Machine Vision Conference*, pages 119.1–119.10. BMVA Press, 2011. http://dx.doi.org/10.5244/C.25.119.

[23] Ville Ojansivu and Janne Heikkilä. Blur insensitive texture classification using local phase quantization. In *International conference on image and signal processing*, pages 236–243. Springer, 2008.

[24] Juho Kannala and Esa Rahtu. Bsif: Binarized statistical image features. In *Pattern Recognition (ICPR), 2012 21st International Conference on*, pages 1363–1366. IEEE, 2012.

[25] Miao Liu, Mingjun Wang, Jun Wang, and Duo Li. Comparison of random forest, support vector machine and back propagation neural network for electronic tongue data classification: Application to the recognition of orange beverage and chinese vinegar. *Sensors and Actuators B: Chemical*, 177:970–980, 2013.

[26] Manuel Fernández-Delgado, Eva Cernadas, Senén Barro, and Dinani Amorim. Do we need hundreds of classifiers to solve real world classification problems? *The Journal of Machine Learning Research*, 15(1):3133–3181, 2014.

[27] HR Sheikh, Z Wang, L Cormack, and AC Bovik. Live image quality assessment database release 2 (2005), 2005.

[28] Eric C Larson and DM Chandler. Categorical image quality (csiq) database. *Online, http://vision. okstate. edu/csiq*, 2010.

[29] Nikolay Ponomarenko, Lina Jin, Oleg Ieremeiev, Vladimir Lukin, Karen Egiazarian, Jaakko Astola, Benoit Vozel, Kacem Chehdi, Marco Carli, Federica Battisti, et al. Image database tid2013: Peculiarities, results and perspectives. *Signal Processing: Image Communication*, 30:57–77, 2015.

[30] Pedro Garcia Freitas, Welington YL Akamine, and Mylène CQ Farias. Referenceless image quality assessment by saliency, color-texture energy, and gradient boosting machines. *Journal of the Brazilian Computer Society*, 24(1):9, 2018.

JOIN US AT THE NEXT EI!

IS&T International Symposium on

Electronic Imaging

SCIENCE AND TECHNOLOGY

Imaging across applications . . . Where industry and academia meet!

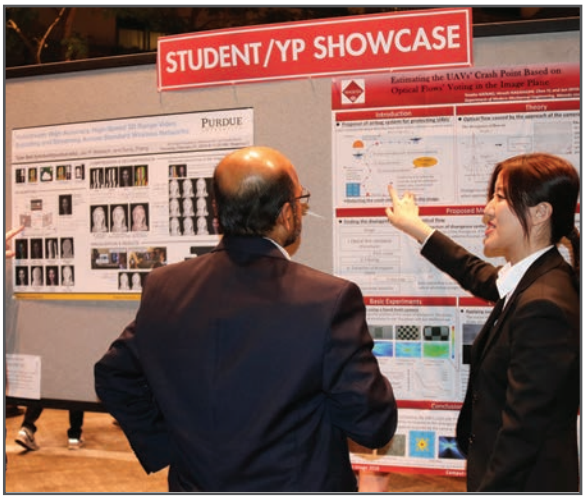

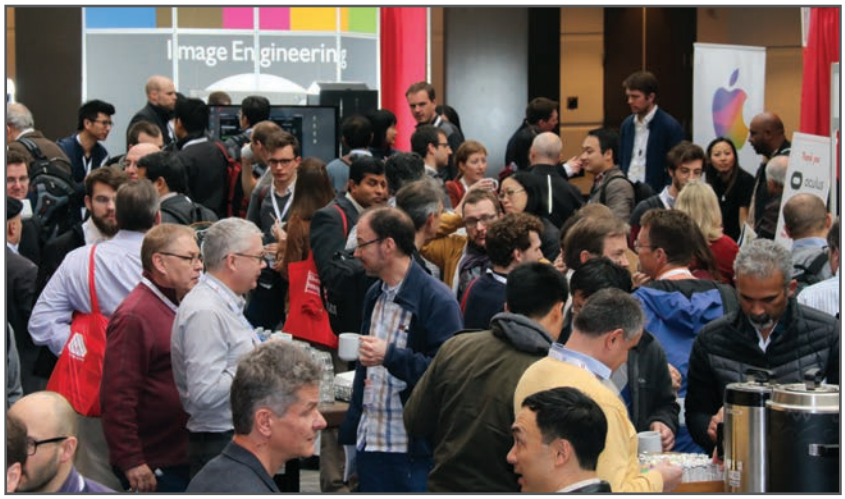

• SHORT COURSES • EXHIBITS • DEMONSTRATION SESSION • PLENARY TALKS •
• INTERACTIVE PAPER SESSION • SPECIAL EVENTS • TECHNICAL SESSIONS •

www.electronicimaging.org

IS&T
imaging.org